Temperature Raman scattering study of CaAlTaO perovskite crystal

T. Runka, M. Berkowski, A. Łapiński, M. Drozdowski

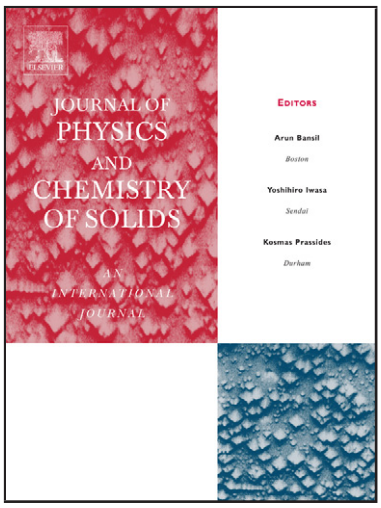

www.elsevier.com/locate/jpcs

Temperature Raman scattering study of $CaAl_{0.5}Ta_{0.5}O_3$ perovskite crystal

T. Runka, M. Berkowski, A. Łapiński, M. Drozdowski

PII: S0022-3697(07)00774-3
DOI: doi:10.1016/j.jpcs.2007.12.011
Reference: PCS 5347

To appear in: *Journal of Physics and Chemistry of Solids*

Received date: 17 September 2007
Revised date: 26 November 2007
Accepted date: 14 December 2007

Cite this article as: T. Runka, M. Berkowski, A. Łapiński and M. Drozdowski, Temperature Raman scattering study of $CaAl_{0.5}Ta_{0.5}O_3$ perovskite crystal, *Journal of Physics and Chemistry of Solids* (2007), doi:10.1016/j.jpcs.2007.12.011

Temperature Raman scattering study of $CaAl_{0.5}Ta_{0.5}O_3$ perovskite crystal

T. Runka[1*], M. Berkowski[2], A. Łapiński[3] and M. Drozdowski[1]

[1]*Faculty of Technical Physics, Poznan University of Technology, ul. Nieszawska 13A, 60-965 Poznań, Poland*

[2]*Institute of Physics, Polish Academy of Sciences, Al. Lotników 32/46, 02-668 Warszawa, Poland*

[3]*Institute of Molecular Physics, Polish Academy of Sciences, ul. Smoluchowskiego 17, 60-179 Poznań, Poland*

Abstract – Temperature Raman scattering studies were performed for $CaAl_{0.5}Ta_{0.5}O_3$ crystal. This material features NaCl type ordering of Al^{3+} and Ta^{5+} ions at the B-site superimposed onto $b^-b^-c^+$ octahedral tilting. Because of existing twin-related domains in crystal structure, the micro-Raman measurements were carried out at room temperature. Some differences in Raman spectra obtained using macro- and micro-Raman system were revealed. Most of the Raman modes show monotonous red-shift with the increase temperature. Only cubic-like fully symmetric A_{1g} mode slightly increases its frequency with increase temperature. There are no uncontinous changes of mode frequency in temperature range studied. It indicates stable character of static distortions of crystal structure relying on changes of octahedra tilt angle.

* Corresponding author. Tel.: +48 61 665 3170; fax: +48 61 665 3164.
E-mail address: tomrun@phys.put.poznan.pl (T. Runka).

Keywords: A. inorganic compounds, C. Raman spectroscopy, D. microstructure

1. Introduction

One of the example of well-ordered perovskites is $CaAl_{0.5}Ta_{0.5}O_3$ crystal (abbreviated as CAT). CAT crystal and its related two- and three-component perovskites are considerably interesting materials due to their application as a substrates for epitaxial deposition of high temperature superconductors (HTSc) [1].

Such as other ABO_3 perovskites, $CaAl_{0.5}Ta_{0.5}O_3$ comprises a three-dimensional framework of corner-sharing B'/B"O_6 octahedra with A cations (Ca in CAT crystal) occupying its cavities (see Fig. 1) [2].

Fig. 1

It is necessary to remind that the ideal ABO_3 perovskite structure is a cubic one with space group symmetry $Pm\bar{3}m$ [3]. It has been assumed the possibility of occurring three different distortions in perovskite structure: i) distortions of BX_6 octahedra; ii) *B*-cation displacements within these octahedra and iii) tilting of BO_6 octahedra relative to one other as corner-linked, practically rigid units. These different kinds of distortions which can occur separately or in combination with possibilities of cations/anions ordering give a lot of possibilities in crystal structure realization [3-6]. In compounds with two different cations in perovskite octahedral sites (e.g. $AB'_{1/2}B''_{1/2}O_3$ compounds), 1:1 ordering of *B*-site cations takes place and a face-centred cubic elpasolite-type structure with $Fm\bar{3}m$ symmetry is created.

The $CaAl_{0.5}Ta_{0.5}O_3$ crystal is isomorphous with $CaAl_{0.5}Nb_{0.5}O_3$ (abbreviated as CAN) crystal because of the ionic radii of Ta^{5+} and Nb^{5+} ions, which are equal to 0.64 Å. The structure of CAT crystal at room temperature was described by Berkowski et al. [1]. The authors have been proposed orthorhombic *Pbnm* space group symmetry with lattice parameters: a = 5.42232 Å, b = 5.37864 Å, c= 7.62962 Å. However, Levin et al. have been proposed precise investigations of CAN crystal (isomorphous structure to CAT) using detailed X-ray diffraction and Transmition Electron Microscope (TEM) study, indicating small deviation to monoclinic $P2_1/n$ structure with unit cell parameters: a = 5.3780(1) Å, b = 5.4154(1) Å, c= 7.6248(2) Å and β = 89.968(2)° [7]. The structure apparently features a superposition of $b^-b^-c^+$ octahedral tilting and B-site cations ordering. In the absence of octahedral tilting, existing B-site cations ordering leads to a cubic structure with $Fm\bar{3}m$ symmetry and lattice parameters equal to $a = 2a_c$ (a_c – simple cubic axis). Levin et al. also discuss microstructure of CAN crystal consisting of twin-related domains representing six crystallographic variants of pseudo-orthorhombic structure with different orientations of the $a \approx \sqrt{2}a_c$, $b \approx \sqrt{2}a_c$ and $c \approx 2a_c$ axes. The tolerance factor of CAN (very similarly for CAT) is 0.972, assuming disordered structure and 12-fold coordination for Ca ions. The ions in the double monoclinic $P2_1/n$ unit cell of CAN occupy Ca – 4e; (Al/Nb)1 – 2b; (Al/Nb)2 – 2c; O(1), O(2) and O(3) – 4e sites [7].

Our previous papers are related to low- and high temperature study of selected crystals with different composition belonging to the tetragonal and orthorhombic symmetry by Raman spectroscopy [8,9].

The aim of this work is the Raman scattering study of CAT crystal in a wide range of temperature from 77 to 620 K. The first part of the paper presents both theoretical predictions of the activity of zero-wave vector phonons (q≈0) for orthorhombic *Pbnm* and monoclinic $P2_1/n$ structure and experimental results of Raman scattering study obtained using macro- and micro-Raman system. A comparison of the experimental Raman data with theoretical analysis was performed in order to identify the structural and order-induced phonon modes. In a second part of the paper the study of temperature-induced changes in Raman spectra caused by static distortions of crystal structure are presented.

2. Experimental

The CAT crystal used in Raman experiment has been grown by the Czochralski method. The growth processes were carried out in an iridium crucible 40 mm in diameter at the pulling rate of 1÷2 mm/h and rotation rate of 20 rpm in a pure nitrogen atmosphere with oxygen concentration in the outlet gas below 1000 ppm. The melting temperature of all these solutions was in the temperature range of 1800-1850 ºC [1].

The Raman investigations of CAT crystal were carried out for oriented sample. The sample of dimensions 4×4×5 mm^3, were cut with the edges parallel to the axes of laboratory co-ordinate system *XYZ*, where $X||a$, $Y||b$ and $Z||c$. The room temperature Raman spectra recorded in $Z(XX)Y$ and $Z(XZ)Y$ scattering geometries are presented in Fig. 2a. As it is seen from this figure they are qualitatively very similar because of twin-domain microstructure of CAT crystal. Due to mentioned reason, the temperature measurements have been carried out for $Z(XZ)Y$ scattering geometry. The crystal was

heated using a home-made heating stage (with temperature stability ± 2 K) in the temperature range 293 – 680 K. The low temperature measurements were carried out in Oxford cryostat in temperature range 77 – 293 K with temperature stability ± 0.1 K. The 100 mW output power of the 488 nm line of an Ar^+ ion laser was used to excite the Raman spectra. The scattered light was collected in 90^o geometry and was analysed by double-grating monochromator equipped with photomultiplier and photon-counting system. The spectra in the range 80 – 1000 cm^{-1} with the spectral slit-width 2 cm^{-1} were recorded. The position of Raman peaks was calibrated using CCl_4 as an external standard. The spectral parameters of Raman bands, such as: wavenumber of the peak centre position, intensity, integral intensity, and FWHM (full width at half maximum) were determined using fitting procedure. All Raman bands were fitted with Lorentzian line shape function. In order to obtain correct intensity of first-order Stokes Raman bands in temperature measurements, all spectra were fitted with the spectral response function: $S(\nu) = S_0(\nu)[1 + n(\nu)]$, where $n(\nu)=1/(e^{h\nu/kT}-1)$ is Bose-Einstein population factor.

Fig. 2

The measurements of polarized Raman spectra at room temperature were performed in back-scattering geometry using a LabRam HR 800 Jobin-Yvon Horiba confocal spectrometer equipped with a liquid-N_2-cooled charge couple device (CCD) and two lasers: Stabilite 2017 (Ar^+ ion laser) and He-Ne. The laser power of 488 nm wavelength, before focusing with 100x objective, was less than 20 mW. The objective 100x ensures the diameter of laser radiation spot approximately equal to 0.66 μm. A

Notch filter was used to stray light rejection. The instrumental resolution was 2 cm^{-1}. The position of Raman peaks was calibrated using Si thin film as an external standard.

3. Group theory analysis of structural Raman-active modes

Group theory predicts for cubic centrosymmetric structure of type $Pm\bar{3}m$, the zone-centre optical phonons of odd-parity ($4F_{1u} + F_{2u}$). It means that there are no Raman-active modes in the first-order vibrational spectrum [10,11].

Assuming ordering of B-site cations in perovskites with two different B', B" ions (ions with different charge and/or size), face-centred cubic superstructure with $Fm\bar{3}m$ symmetry is created (elpasolite-type structure). The primitive unit cell contains two structural units, giving a total of 30 normal modes at q≈0. The site symmetry group analysis performed for $Fm\bar{3}m$ space group leads to following irreducible representation:

$$\Gamma = A_{1g}(R) + E_g(R) + 2F_{2g}(R) + F_{1g}(s) + 4F_{1u}(IR) + F_{2u}(s) + F_{1u}(ac)$$

The elpasolite-type structure crystals are known to give rise to intense Raman signal. The A_{1g} and F_{2g} modes are usually very strong in Raman spectrum, and E_g mode is detected as a weak one [10,11].

The group theory calculations performed for orthorhombic *Pbnm* structure predict activity of the following modes:

$$\Gamma = 7A_g(R) + 7B_{1g}(R) + 5B_{2g}(R) + 5B_{3g}(R) + 8A_u(s) + 7B_{1u}(IR) + 9B_{2u}(IR) + 9B_{3u}(IR)$$

$\Gamma_{ac.} = B_{1u} + B_{2u} + B_{3u}$,

where: R – Raman-active modes, IR – infrared active modes, ac – acoustic modes and s – silent modes.

Among all of 60 normal modes predicted by theory only 24 are Raman-active ($7A_g$ + $7B_{1g}$ + $5B_{2g}$ + $5B_{3g}$) [8].

Exclusively concentrating on Raman-active modes and assuming $P2_1/n$ crystal structure with the same volume of primitive unit cell, group theory calculations predicts also the activity of 24 modes from which twelve have A_g symmetry and twelve B_g symmetry. The correlation of Raman-active modes between elpasolite-type structure ($Fm\bar{3}m$), cubic ($Pm\bar{3}m$), orthorhombic (*Pbnm*) and monoclinic ($P2_1/n$) structure is shown in Fig. 3 [12].

Fig. 3

4. Results and discussion

First of all, in this paper, we present the temperature-dependent studies of CAT crystal possessing orthorhombic *Pbnm* space group. We also present preliminary measurements of polarized Raman spectra performed using micro-Raman experimental system. This point have been appeared because conventional measurements (macro-Raman) of CAT crystal in different sample configurations gave practically the same Raman spectra (see Fig. 2a). Normalized micro-Raman spectra of CAT crystal in proper polarizations are presented in Fig. 2b. Comparing the spectra obtained in (XX) and (XZ)

polarization, carried out in macro- and micro-Raman system, we revealed some changes in bands intensities. The most essential differences are seen in the spectral range 200 – 520 cm^{-1}. The strongest changes in polarization of vibrations were noticed in the region of deformation vibration of oxygen octahedra. Changes in the intensity ratio for this triply degenerate mode for two different polarizations (XX) and (XZ) indicate different symmetry of individual components of this mode (see Fig. 4).

Fig. 4

Comparing also the spectra obtained for (XX) and (XY) polarization we ascertain that mode positioned at 476 cm^{-1} can be assigned to A_g symmetry, mode centred at 483 cm^{-1} can be assigned to B_{1g} symmetry. The third component located at 488 cm^{-1} is assigned to B_{2g} symmetry and is observed with comparable intensity in different scattering geometries. It is also worth to remark some changes in the intensities for modes in the spectral range 350 – 390 cm^{-1} and 210 – 230 cm^{-1} for different scattering geometries. Remaining modes are not sensitive on change of scattering geometry. There are no fully polarized modes in Raman spectrum, i.e. all of modes are more or less depolarized. So, we can conclude that differences in polarized spectra performed using macro- and micro-Raman system indicate existing of unsimilarity in crystal structure, e.g. microstructure consisting of twin-related domains.

The Raman spectra obtained for selected temperatures are presented in Fig. 5. Taking into account the Raman spectrum obtained at LN temperature, one can noticed that the number of experimentally observed Raman modes is lower than theoretically predicted by factor group analysis. Only 16 modes of 24 expected are detected in

Raman spectrum. The assignment of the Raman modes will be referred to ordered elpasolite-type structure. The strong, prominent modes of A_{1g}, E_g and $F_{2g}(2)$ cubic-like symmetry appearing in the spectral range above 400 cm^{-1} are attributed to internal vibrations of oxygen octahedra. The narrow $F_{2g}(2)$ mode of highest intensity centered at about 481 cm^{-1} appears from bending vibration of octahedra, weaker broad mode at 856 cm^{-1} is assigned to symmetric stretching vibration of A_{1g} symmetry, and the least intensive mode positioned at about 580 cm^{-1} is attributed to asymmetric stretching vibration E_g. Low frequency region of Raman spectrum is dominated by lattice modes which originate from translational and librational vibrations of Ca^{2+} and B'/B"O_6 ions.

Fig. 5

Prosandeev et al. presented computational calculations of Raman intensities for the complex perovskites from the first principles [13]. They performed calculations for a double perovskite $CaAl_{0.5}Nb_{0.5}O_3$ crystal. Because the CAN and CAT crystals are isomorphous we decided to compare our experimental data with their first-principles computations. The authors performed their calculations for two structures: i) ordered cubic elpasolite-type structure $Fm\bar{3}m$, and ii) monoclinic structure $P2_1/n$, considering octahedral tilting and cations ordering at the B-site. The detailed results of the first-principles computations for cubic $Fm\bar{3}m$ (no tilting) and monoclinic $P2_1/n$ (tilting) structure of CAN are given in the paper [13]. The relative intensities and frequency obtained in both the computation for CAN and our experimental results for CAT obtained at RT are listed in Table 1.

Table 1

The Raman spectra computed for tilted ($P2_1/n$) and untilted ($Fm\bar{3}m$) CAN crystal reveal significant differences, especially in the lattice modes region. Triply degenerate F_{2g} modes split in the low-symmetry structure into three lines and shift to higher frequencies. This shift is significant for the low frequency lattice mode and insignificant for internal bending vibrational mode.

Levin et. al experimentally recorded for CAN crystal three strong sharp spectral features at 480, 550, and 850 cm^{-1} [7]. As it can be seen from Table 1, we observe for CAT crystal the bands at around 481, 580, and 856 cm^{-1} which correspond to these obtained by Levin et. al. For the triply degenerate mode at around 481 cm^{-1} we have served the average value of wavenumber calculated from its three components. Small difference in wavenumber value is related to type of ion in the centre of oxygen octahedron (Nb^{5+}, Ta^{5+}). However, in case of deformation vibration E_g the change in wavenumber is quite large reaching the value 30 cm^{-1}. Similar effect concerning the shift of A_{1g} and E_g modes when Nb^{5+} ion is substituted by Ta^{5+} ion was also observed by Tao et. al for $SrAl_{0.5}Nb_{0.5}O_3$ and $SrAl_{0.5}Ta_{0.5}O_3$ (abbreviated in literature as SAN and SAT, respectively) elpasolite-type structure crystals [14]. However, frequency shift evoked by substitution effect when Nb^{5+} was replaced by Ta^{5+} for SAN and SAT is stronger. In this case the change in wavenumber obtained by authors was 37 cm^{-1} and 15 cm^{-1} for E_g and A_{1g} mode, respectively. It is also known from the literature that such a substitution does not significantly influence the position of deformation F_{2g} mode [11,14,15].

Temperature study of CAT crystal

The Raman spectra obtained at several temperatures are presented in Fig. 5. The spectra inserted in this figure are experimental spectra corrected for the Bose-Einstein temperature factor. The theoretical calculations for CAN proposed by Prosendeev predict that triply degenerate cubic mode $F_{2g}(1)$ splits into three modes positioned at 188 cm^{-1}, 211 cm^{-1} and 242 cm^{-1} in monoclinic structure [13]. These modes are attributed to translational motions of Ca^{2+} cation. In CAT crystal we observe three modes with comparable wavenumber values. The temperature dependence of wavenumber for lattice modes is presented in Fig. 6.

Fig. 6

The strongest temperature changes in wavenumber we observe for modes centred at about 160 cm^{-1} and 280 cm^{-1} (the position is given for LN temperature). All lattice modes show monotonous change in wavenumber while temperature increasing, except for the mode positioned at about 170 cm^{-1} that increases slightly its wavenumber in the temperature range 250 – 350K and mode at about 210 cm^{-1} which is completely temperature insensitive. The temperature dependence of three low intensive modes in the middle-wavenumber range 300 – 400 cm^{-1} is shown in Fig. 6. These modes are distinctly separated below RT but in higher temperatures they merge into very broad band. However, three-component structure of this band is conserved at the highest temperatures as well. The triplet in the frequency range 470 – 490 cm^{-1} attributed to cubic-like $F_{2g}(2)$ mode shows a weak temperature changes in wavenumber in

temperature range form LN to RT and a little bit stronger above RT. An extra mode near the $F_{2g}(2)$ triplet positioned at about 510 cm^{-1} (at LN temperature) shows 5cm^{-1} red-shift when the temperature increase to 620 K. The temperature dependence of modes recorded in spectral range 460 – 520 cm^{-1} is presented in Fig. 7.

Fig. 7 and Fig. 8

The other two high-frequency modes E_g and A_{1g} attributed to asymmetric and symmetric stretching vibrations of oxygen octahedra, respectively, show different temperature dependence (see Fig. 7). Lower frequency E_g mode changes slightly its frequency in temperature range from LN to RT and shows stronger (about 10 cm^{-1}) red-shift in temperature range between RT and 620K. The highest frequency cubic-like A_{1g} mode is only one mode that shows small blue-shift in whole temperature range studied. Both stretching modes strongly decrease their intensity with increasing temperature. Large increase of FWHM with the increase temperature is observed for all modes in spectrum. The temperature depenedence of FWHM for selected A_{1g} and E_g modes is presented in Fig. 8.

5. Conclusions

The micro-Raman measurements at RT and temperature-dependent conventional investigations of CAT crystal were carried out. The differences in room temperature spectra obtained using micro-Raman and conventional experimental system (macro-Raman) were revealed. The observed number of Raman-active modes in the spectrum is

lower than theoretically predicted assuming orthorhombic as well as monoclinic structure of CAT crystal. The measured spectra possess characteristic spectral features for elpasolite-type structure crystals. Most of the Raman modes show red-shift of frequency with increasing temperature with except for A_{1g} cubic-like mode which increases its frequency. With the increase temperature two modes positioned at 160 and 280 cm^{-1} show great shift equal to 30 and 33 cm^{-1}, respectively. Finally, we can conclude that monotonous changes in spectral parameters of Raman bands of crystal being under study indicate static changes of distorted crystal structure with temperature

Acknowledgments

This work was supported in part by Research Project of Poznan University of Technology No. 64-001/07.

References

1. M. Berkowski, R. Aleksiyko, J. Fink-Finowicki, R. Diduszko, P. Byszewski, R. Kikaleshvili-Domukhovska, J. Cryst. Growth 269 (2004) 512–517.
2. Diamond Version 2.1c (Visual Crystal Structure Information System).
3. H.D. Megaw, Crystal Structures: A Working Approach. W.B. Saunders Co., Philadelphia, Pa., 1973.
4. C.J. Howard, H.T. Stokes, Acta Cryst. B60 (2004) 674–684.
5. A.M. Glazer, Acta Cryst. B28 (1972) 3384–3392.
6. P. Woodward, Acta Cryst. B53 (1997) 32–43.
7. I. Levin, J.Y. Chan, J.E. Maslar, T.A. Vanderah, S.M. Bell, J. Appl. Phys. 90 (2001) 904–914.
8. T. Runka, M. Berkowski, M. Drozdowski, J. Mol. Structure 792-793 (2006) 221–226.
9. T. Runka, M. Berkowski, M. Drozdowski, J. Mol. Structure – Article in Press DOI: 10.1016/j.molstruc.2007.05.047.
10. T. Runka, K. Łapsa, A. Łapiński, R. Aleksiyko, M. Berkowski, M. Drozdowski, J. Mol. Structure 704 (2004) 281–285.
11. G. Siny, R. Tao, R.S. Katiyar, R. Guo, A.S. Bhalla, J. Phys. Chem. Solids 59 (1998) 181–195.
12. M. Zaghrioui, A. Bulou, P. Lacorre, P. Laffez, Phys. Rev. B 64 (2001) 081102-1–081102-4.
13. S.A. Prosandeev, U. Waghmare, I. Levin, J. Maslar, Phys. Rev. B 71 (2005) 214307-1–214307-9.

14. R. Tao, A.R. Guo, C.-S. Tu, I. Siny, R.S. Katiyar, R. Guo, A.S. Bhalla, Ferroelectrics Letters 21 (1996) 79–85.

15. R. Ratheesh, M. Wöhlecke, B. Berge, Th. Wahlbrink, H. Haeuseler, E. Rühl, R. Blachnik, P. Balan, N. Santha, M.T. Sebastian, J. Appl. Phys. 88 (2000) 2813–2818.

Figure Captions

Fig. 1. The crystal structure of $CaAl_{0.5}Ta_{0.5}O_3$.[2]

Fig. 2. Room temperature spectra of $CaAl_{0.5}Ta_{0.5}O_3$ crystal obtained by using: a) conventional measurements (macro-Raman); b) micro-Raman measurements.

Fig. 3. Correlation diagram of Raman-active modes considering mode symmetry relations between elpasolite ($Fm\bar{3}m$), cubic ($Pm\bar{3}m$), orthorhombic (*Pbnm*) and monoclinic ($P2_1/n$) structure. X, M, R refers to different points of the Brillouin zone of $Pm\bar{3}m$ cubic structure.

Fig. 4. The micro-Raman spectra from the region of bending vibrations of oxygen octahedra measured in $Y(XX)\bar{Y}$, $Y(XZ)\bar{Y}$ and $Z(XY)\bar{Z}$ scattering geometry. Dots mark experimental data points, solid lines mark curvefiting line and four components being result of fitting procedure.

Fig. 5. The Raman spectra of $CaAl_{0.5}Ta_{0.5}O_3$ crystal obtained for selected temperatures.

Fig. 6. The temperature dependence of wavenumber for mode from the spectral range 50 – 400 cm^{-1}.

Fig. 7. The temperature dependence of wavenumber for internal vibrational modes of oxygen octahedral.

Fig. 8. The temperature dependence of FWHM for A_{1g} and E_g modes.

Table 1

The wavenumbers and relative intensities obtained in the first-principles computation for CAN crystal assuming $Fm\bar{3}m$ and $P2_1/n$ space group. The asterisks indicate modes calculated for $P2_1/n$ which are closest to those obtained for $Fm\bar{3}m$ structure . Last column contains our experimental results obtained in our study for CAT crystal at room temperature

	CAN [13]				CAT [this work]
	$Fm\bar{3}m$		$P2_1/n$		$Pbnm$
Mode symmetry in cubic structure	$\omega_{calc.}$ (cm^{-1})	$I^{crystal}$	$\omega_{calc.}$ (cm^{-1})	I^{powder}	$\omega_{exp.}$ (cm^{-1})
A_{1g}	910	8.7388	797*	1.2048	856 s
E_g	660	2.8332	554*	0.0200	580 m
			553*	0.0249	
F_{2g}	445	4.9791	457*	0.3368	487 s
			452*	0.2971	481 s
			446*	0.2526	474 s
			242*	0.0534	246 m
			211*	0.0296	211 w
F_{2g}	101	11.8411	188*	0.0565	181 w
			770	0.0008	
			351	0.0026	356 w
			732	0.0047	
			482	0.0312	508 w
			289	0.0000	273 w
			331	0.0281	341 w
			237	0.0126	224 w
			359	0.0197	382 w
			564	0.0052	

185	0.0045	
175	0.282	171w
136	0.0186	
182	0.0032	
162	0.0105	151w
339	0.0104	

Where: s – strong, m – medium, w – weak.

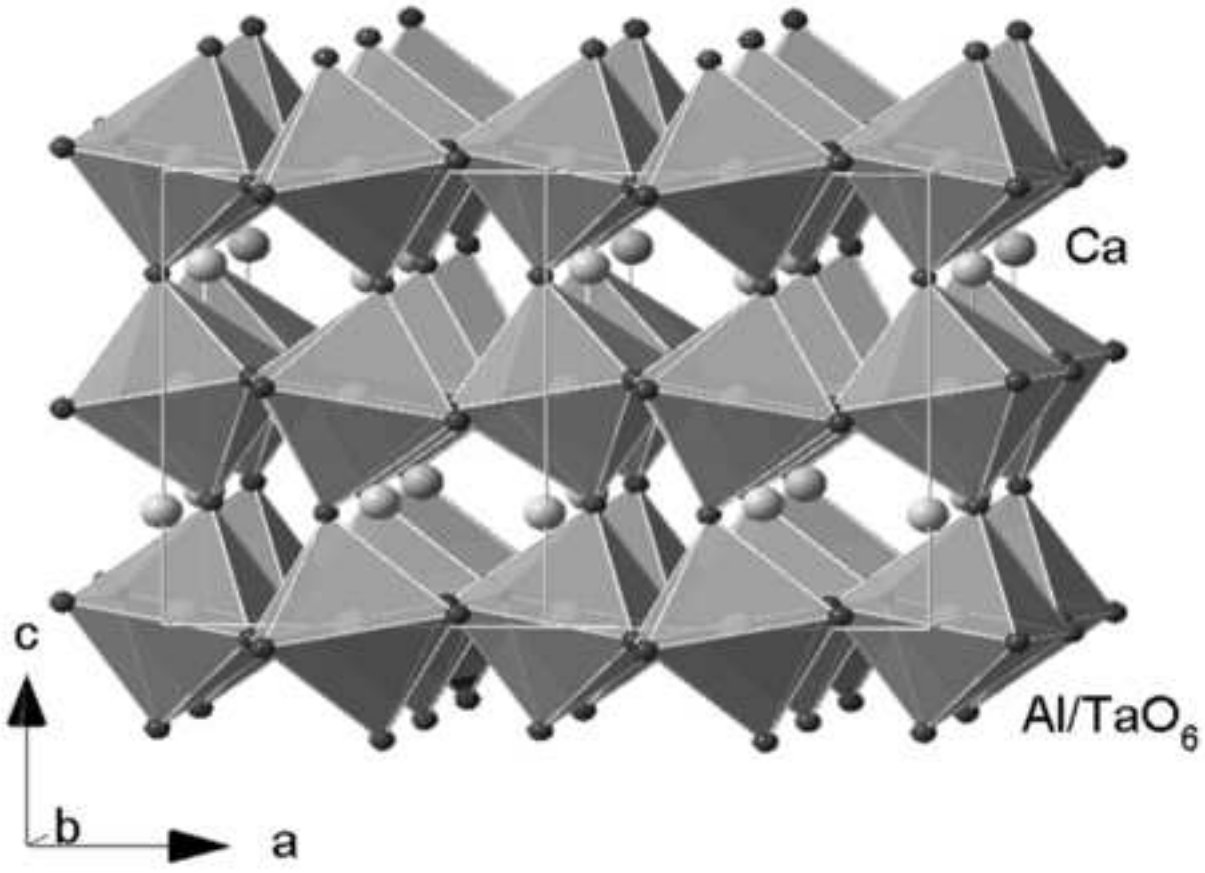

Figure2

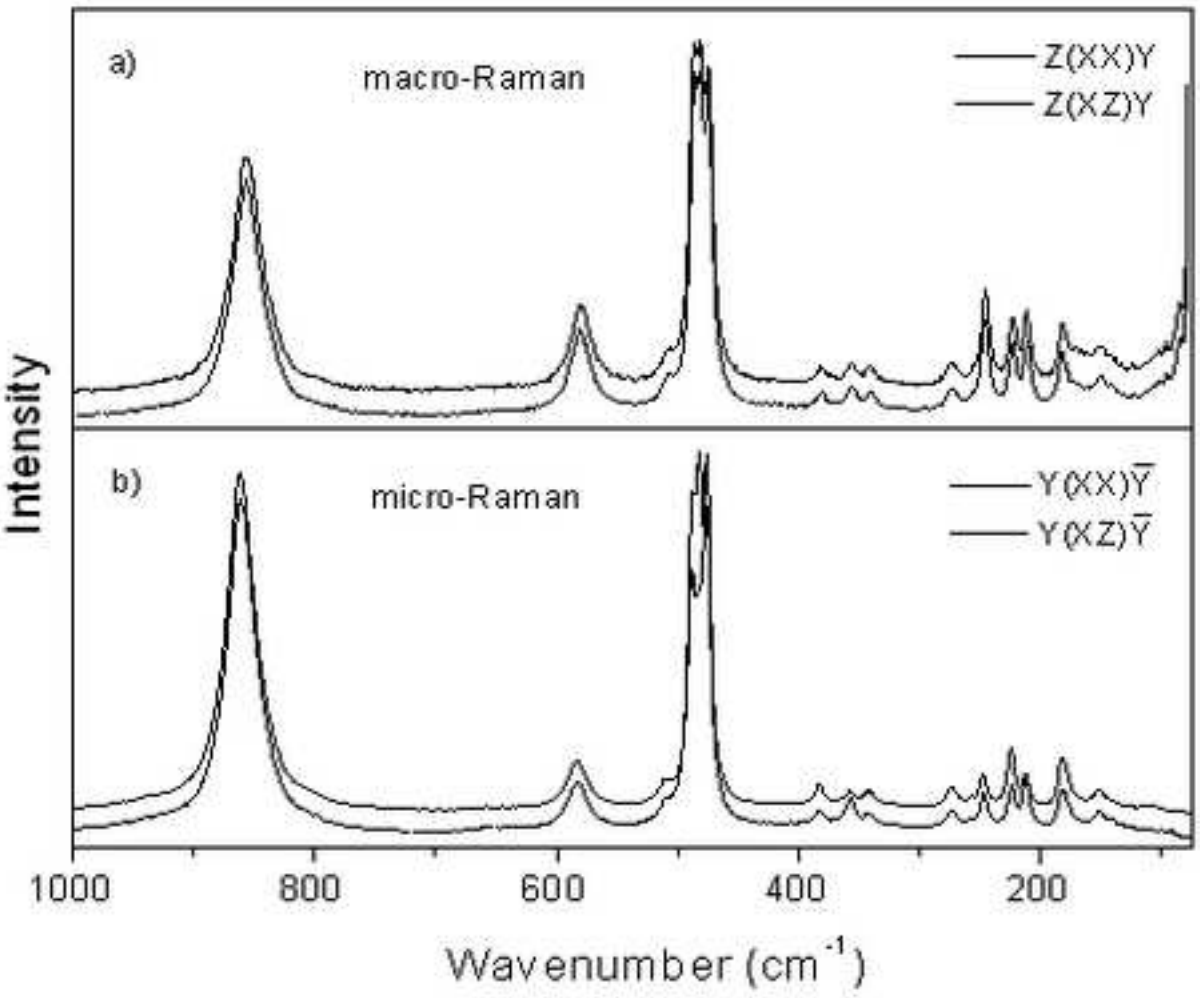

Figure3

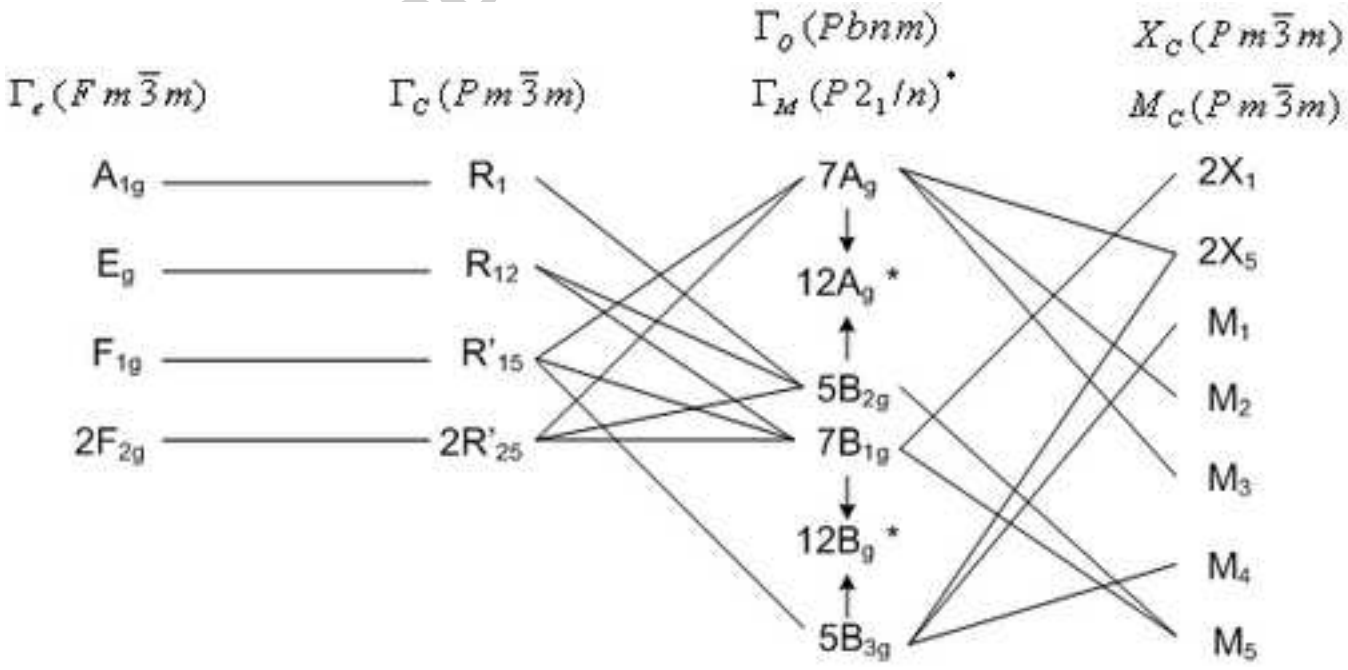

Figure4

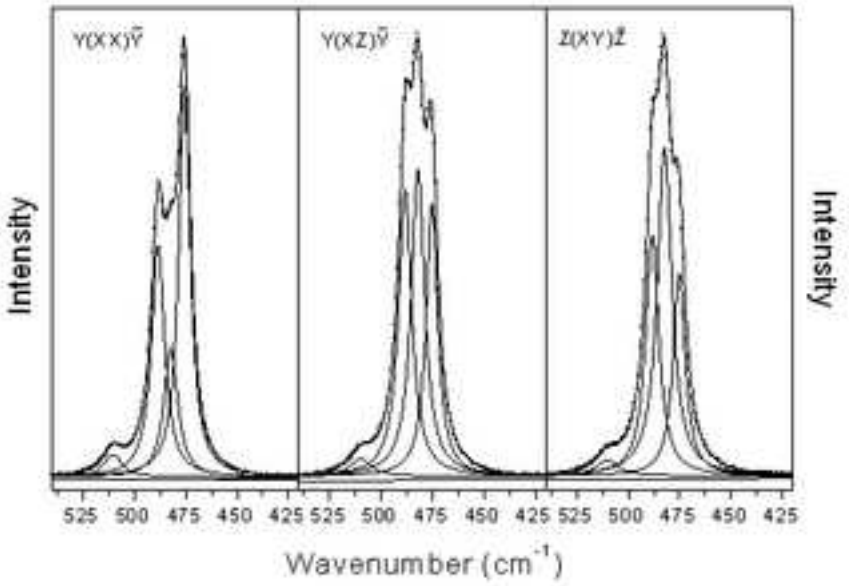

Figure5

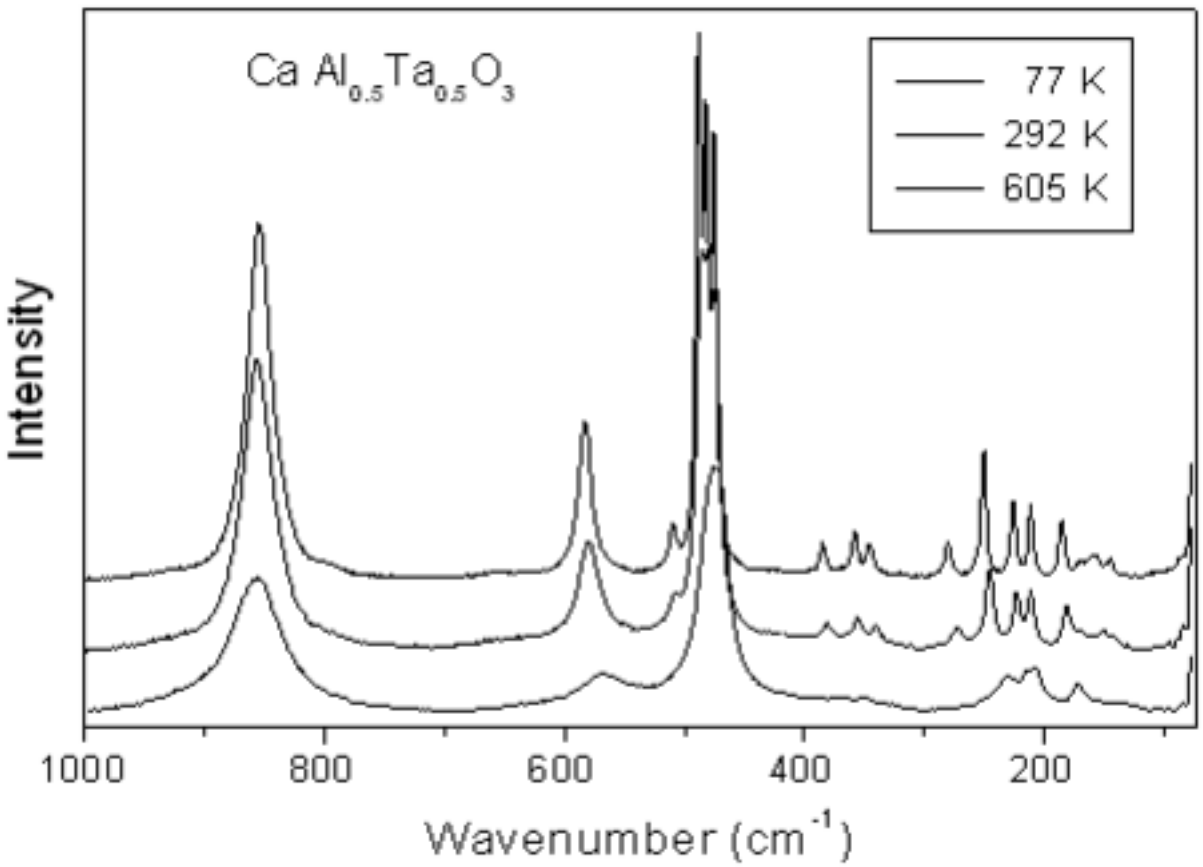

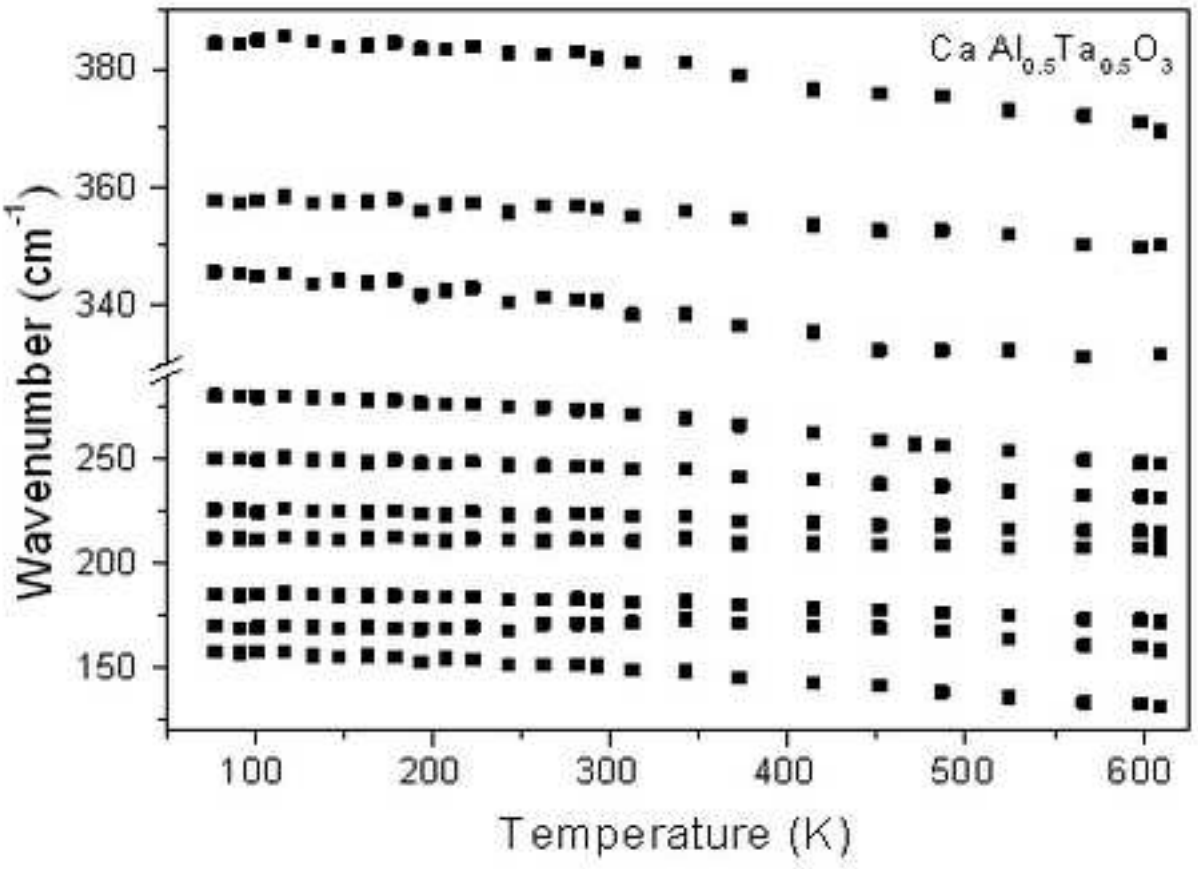

Figure7

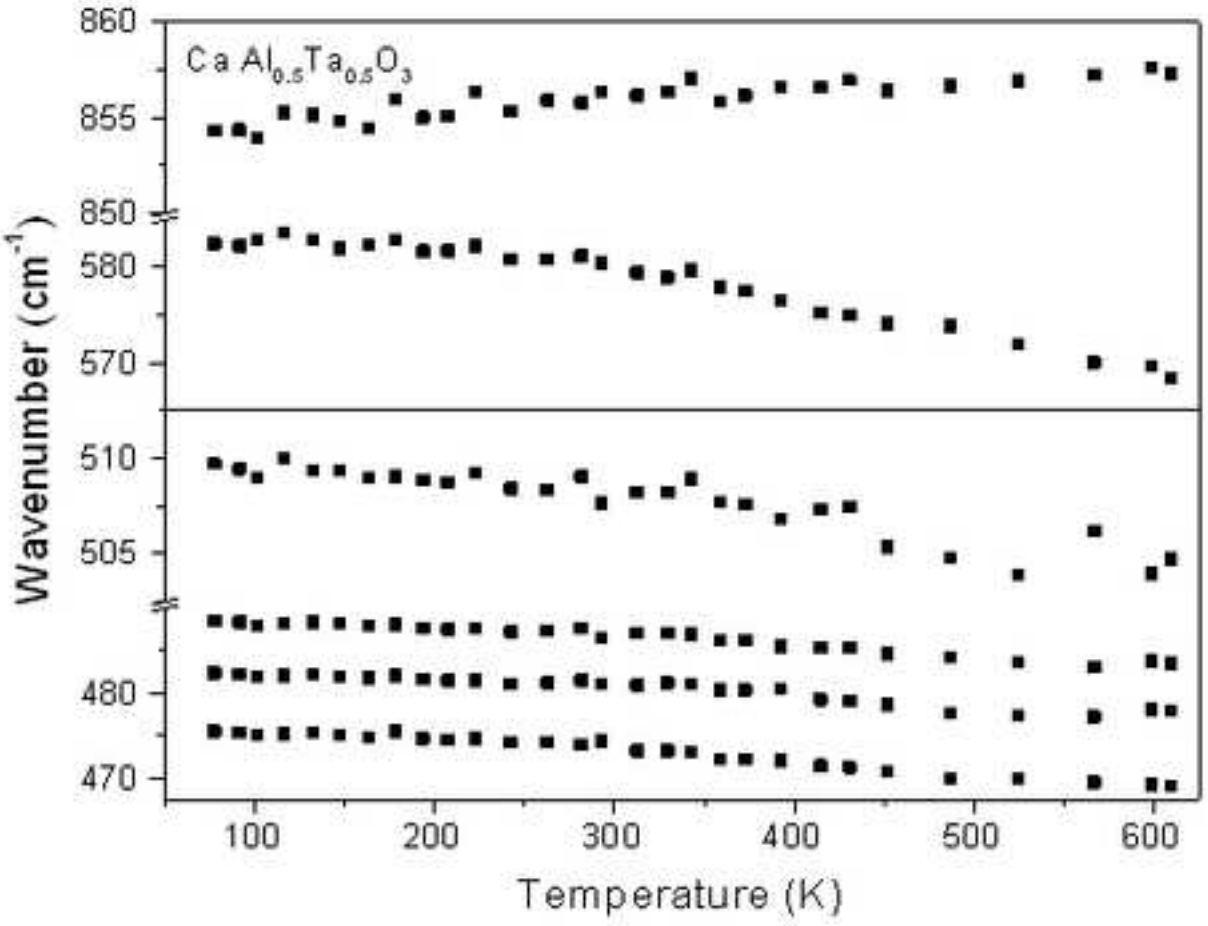

Figure8